Numerical Design of a Gain-Switched Pulsed Laser at 3.92 μm Wavelength Based on a Ho^{3+}-Doped Fluoroindate Fiber

Antonella Maria Loconsole, Mario Christian Falconi, Vincenza Portosi, and Francesco Prudenzano, *Member, IEEE*

***Abstract*—A gain-switched pulsed laser based on a commercial, heavily holmium-doped fluoroindate glass fiber, is designed to emit in the middle-infrared range, at the wavelength $\lambda = 3.92\ \mu$m. The laser, pumped at $\lambda = 888$ nm, is modeled by a six-level system, by taking into account experimental spectroscopic parameters, to identify a feasible laser configuration. An output signal peak power of about $P_s^{peak} = 14.62$ W with a full width at half maximum (FWHM) pulse duration less than $\tau_s = 73\ ns$ and pulse energy $E_s = 1.214\ \mu$J is predicted, by considering an input peak power of $P_p^{peak} = 10$ W, and pump repetition rate of $f = 100$ kHz, by employing a 8 cm-long fluoroindate fiber with holmium concentration $N_{Ho} = 100\,000$ ppm. The obtained result encourages the construction of a pulsed laser based on commercially available optical fiber, for applications in different fields as sensing and biomedicine.**

***Index Terms*—Electromagnetic design, fiber laser, fluoroindate glass, gain switching, holmium, middle infrared.**

I. Introduction

PULSED lasers in the middle-infrared (Mid-IR) wavelength range find wide application in several fields, including free-space communications, remote sensing, biological sensing, medical diagnostics and surgery, agri-food and environmental monitoring since many chemical molecules show Mid-IR absorption [1]–[8]. Those potential applications have attracted great research interest towards fiber lasers emitting at wavelengths beyond 3 μm. During the recent years, a huge quantity of fiber lasers has been constructed by using different host materials which include silica, germanate, tellurite, ZBLAN or fluoroindate glasses. These glasses have been doped/co-doped with different rare-earth ions such as erbium, ytterbium, dysprosium, thulium, holmium, and praseodymium, to obtain emission at different wavelengths [9]–[13]. Great research interest was focused on Er^{3+}-doped fluoride fiber, since emission at about $\lambda = 2.8\,\mu$m and $\lambda = 3.5\,\mu$m allowed to obtain intriguing laser in continuous wave (CW), gain-switched, and Q-switched regime [14]–[16]. In particular, in [15] a gain-switched fiber laser operating near $\lambda = 3.5\ \mu$m via a dual-wavelength pumping scheme was obtained in an erbium-doped fluorozirconate fiber, with stable pulses with repetition rates ranging between 15 and 20 kHz and laser efficiency of $\eta = 4.7\%$. Fluoroindate optical fibers can exhibit attenuation much smaller with respect to the fluoride ones at longer wavelength, beyond $\lambda = 3.3/3.5\ \mu$m, also with reference to available on market products [17]. They exhibit very promising performances in terms of high transparency, with reduced optical attenuation $\alpha \approx 0.2\,\mathrm{dB/m}$ from ultra-violet (UV) to Mid-IR range [18]. Therefore, they can enable promising applications in the $3 - 5\ \mu$m atmospheric transparency window and in an important part of the molecular fingerprint region. During the last years, rare-earth doped fluoroindate glasses have been spectroscopically investigated with the aim of finding new pumping schemes and operating wavelengths [19]–[24]. As an example, dysprosium and holmium ions allow emission at wavelengths beyond 3 μm [12], [25]. Recently, holmium-doped fluoroindate fibers have been characterized [25]–[29] and CW lasers emitting at $\lambda_s = 2.875\ \mu$m [30] and $\lambda_s = 3.92\ \mu$m [31], [32], pumped at $\lambda_p = 1120\ nm$ and $\lambda_p = 888\ nm$ respectively, have been demonstrated. For that pertaining the pulsed laser operation, emissions at the wavelength $\lambda_s = 2.106\ \mu$m [33] and in the $\lambda_s = 2.95 - 3.015\,\mu$m range [34] have been obtained. The literature results reported in [28]–[31], showing the feasibility of CW laser emission in holmium-doped fluoroindate optical fibers, encourage the investigation/ prediction of the pulsed operation with these optical fibers as an alternative to erbium-doped fluoride ones [15], [16].

In this work, for the first time to the best of our knowledge, the design of a heavily holmium-doped fluoroindate fiber, pumped at $\lambda_p = 888\ nm$, is proposed to obtain laser pulses at $\lambda_s = 3.92\ \mu$m. By using a homemade numerical solver, the pulsed laser behavior is realistically investigated and optimized, employing measured spectroscopic parameter taken from literature [28], [29]. The developed numerical solver is well validated. The employed design approach is similar to that used in [8], where a gain-switched pulsed laser, based on a Dy^{3+}:ZBLAN fiber was suggested and then successfully constructed exploiting

Manuscript received January 4, 2021; revised February 26, 2021; accepted February 27, 2021. Date of publication March 9, 2021; date of current version May 16, 2021. This work was supported by the projects: POR FESRFSE 2014-2020 Innonetwork "Sinach – Integrated systems for mininvasive surgical navigation" – n. BLNGWP7; PON R&I 2014-2020 "New Satellites Generation components - NSG" – Cod. Id. ARS01_01215 NSG; MIUR "Agriculture Green & Digital – AGREED", PNR 2015 – 2020, n. ARS01_00254; EU H2020 "PASSEPARTOUT". *(Corresponding author: Francesco Prudenzano.)*

The authors are with the Department of Electrical and Information Engineering, Politecnico di Bari, 70125 Bari, Italy (e-mail: antonellamaria.loconsole@poliba.it; mariochristian.falconi@poliba.it; vincenza.portosi@poliba.it; francesco.prudenzano@poliba.it).

Color versions of one or more figures in this article are available at https://doi.org/10.1109/JLT.2021.3064764.

Digital Object Identifier 10.1109/JLT.2021.3064764

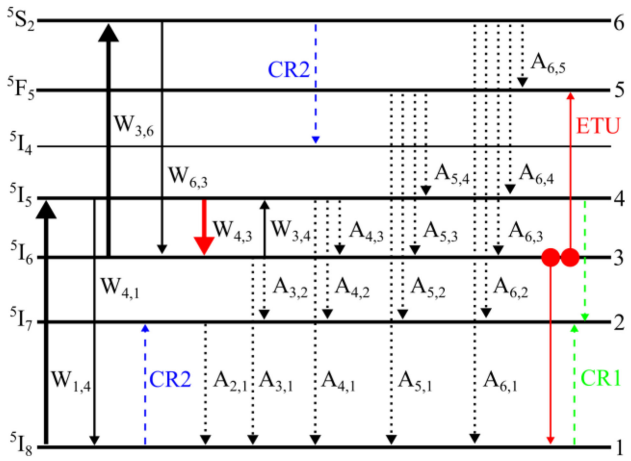

Fig. 1. Energy level scheme for the 6-level laser, pumped at $\lambda_p = 888\ nm$, including pump absorption (transition 1-4, bold black line) stimulated emission at $\lambda_s = 3920\ nm$ (transition 4-3, bold red line), radiative and nonradiative decays (dotted lines), excited state absorption (ESA) (transition 3-6, bold black line), cross-relaxation (CR) (blue and green dashed lines), and energy transfer up-conversion (ETU) (red solid lines).

the same laser transition, even if the pumping wavelength was different [35], [36], with a good agreement between simulation and experimental results. The obtained results are interesting since, until now, only CW laser based on the same commercial Ho^{3+}-doped flouroindate fiber, has been designed [32] or fabricated [31]. Moreover, the practical interest of this work lies in the need of fulfilling accurately the optimized laser parameters identified in the proposed design, in order to construct a pulsed laser in the stable single pulse regime based on a commercial fiber. The simulated performance, in term of laser efficiency are comparable with those obtained by considered other promising dopants and glasses, e.g., the erbium doped fluorozirconate fibers reported in [15].

II. Recall of Theory

The Ho^{3+}-doped fluoroindate fiber stimulated emission at $\lambda_s = 3.92\ \mu$m can be modeled by considering a six-levels system [29], pumped at $\lambda_p = 888\ nm$. The complete level scheme, including all the main phenomena, is reported in Fig. 1. The six-level model is employed instead of the five-level model proposed in [28], [31] because it allows an accurate simulation. It is validated by simulating the CW laser presented in [31], obtaining results in good agreement, as reported in the next section, while the five-level model is not suitable and wrong results are obtained in the cases here investigated. Level $^5I_4$ and level $^5I_5$ degenerate and are considered as single level 4 as reported in [28], [29]. The energy transfer up-conversion phenomenon between level 1 and level 3, starting from level 2, even if included in the model of [29], is here neglected since this approximation does not affect the simulation results. The other light-rare earth interactions taken into account are pump absorption, stimulated emission, radiative and nonradiative decays, excited state absorption (ESA), cross-relaxation (CR), and energy transfer up-conversion (ETU) due to the high Ho^{3+} ions concentration that will be simulated.

By following the rate equations approach [11], [13], [37], the energy level populations $N_1, \ldots, N_6$ can be written as a nonlinear system,

$$\frac{\partial N_1}{\partial t} = -W_{14}N_1 + W_{41}N_4 + A_{61}N_6 + A_{51}N_5 + A_{41}N_4 + A_{31}N_3 + A_{21}N_2 + KN_3^2 - W_{CR1}N_1N_4 - W_{CR2}N_1N_6 \quad (1a)$$

$$\frac{\partial N_2}{\partial t} = -\frac{1}{\tau_{R2}}N_2 + A_{62}N_6 + A_{52}N_5 + A_{42}N_4 + A_{32}N_3 + 2W_{CR1}N_1N_4 + W_{CR2}N_1N_6 \quad (1b)$$

$$\frac{\partial N_3}{\partial t} = -W_{36}N_3 + W_{63}N_6 + W_{43}N_4 - W_{34}N_3 - \frac{1}{\tau_{R3}}N_3 + A_{63}N_6 + A_{53}N_5 + A_{43}N_4 - 2KN_3^2 \quad (1c)$$

$$\frac{\partial N_4}{\partial t} = W_{14}N_1 - W_{41}N_4 - W_{43}N_4 + W_{34}N_3 - \frac{1}{\tau_{R4}}N_4 + A_{64}N_6 + A_{54}N_5 - W_{CR1}N_1N_4 + W_{CR2}N_1N_6 \quad (1d)$$

$$\frac{\partial N_5}{\partial t} = -\frac{1}{\tau_{R5}}N_5 + A_{65}N_6 + KN_3^2 \quad (1e)$$

$$\frac{\partial N_6}{\partial t} = W_{36}N_3 - W_{63}N_6 - \frac{1}{\tau_{R6}}N_6 - W_{CR2}N_1N_6 \quad (1f)$$

where $A_{i,j} = \frac{\beta_{i,j}}{\tau_{Ri}}$ take into account radiative and non-radiative decays, $\beta_{i,j}$ are the branching ratios, τ_{Ri} are the i-th level lifetimes, K is the ETU rate, and W_{CR1} and W_{CR2} are the cross-relaxation transition rates. The condition $N_1 + N_2 + N_3 + N_4 + N_5 + N_6 = N_{Ho}$ is considered, where N_{Ho} is the dopant concentration. The transition rate $W_{i,j}$ for the $i \rightarrow j$ transition is defined as

$$W_{i,j}(z,t) = \frac{\sigma_{i,j}(\lambda_{p/s})}{\frac{hc_0}{\lambda_{p/s}}}[P_p(z,t)]\, i_{p/s}(x,y) \quad (2)$$

where $\sigma_{i,j}(\lambda_{p/s})$ is the cross section at the wavelength $\lambda_{p/s}$ for the $i \rightarrow j$ transition, h is the Plank constant, c_0 is the light speed in vacuum, $\lambda_{p/s}$ is the pump/signal wavelength, $P_p^{\pm}$ is the forward/backward pump power, $P_s^{\pm}$ is the forward/backward signal power, i_p and i_s are the normalized transverse intensity profiles, i.e., the squared modulus of the electromagnetic field, of pump and signal beams, respectively.

The power propagation for pump and signal beams is considered by the following partial differential equations

$$\frac{\partial P_p}{\partial z} + \frac{1}{v_g^p}\frac{\partial P_p}{\partial t} = [g_p(z,t) - \alpha]\, P_p(z,t) \quad (3a)$$

$$\frac{\partial P_s^{\pm}}{\partial z} \pm \frac{1}{v_g^s}\frac{\partial P_s^{\pm}}{\partial t} = \pm[g_s(z,t) - \alpha]\, P_s^{\pm}(z,t) \pm 2h\nu_s B_{ase}\sigma_{43}n_{4s}(z,t) \quad (3b)$$

where

$$g_p(z,t) = -\sigma_{14}(\nu_p)\, n_{1p}(z,t) + \sigma_{41}(\nu_p)\, n_{4p}(z,t) - \sigma_{36}(\nu_p)\, n_{3p}(z,t) + \sigma_{63}(\nu_p)\, n_{6p}(z,t),$$

$$g_s(z,t) = -\sigma_{34}(\nu_s)\, n_{3s}(z,t) + \sigma_{43}(\nu_s)\, n_{4s}(z,t),$$

are the gain coefficients for the pump and the signal, respectively, α is the glass optical loss, v_g^p and v_g^s are the group velocity for the pump and the signal, respectively, and B_{ase} is the equivalent noise bandwidth for the Amplified Spontaneous Emission (ASE), $n_{i,p/s}$ are the overlap integrals over the rare earth-doped region Ω_d between the i-th level population distribution $N_i(x,y,z,t)$ and the pump/signal optical mode intensity $i_{p/s}(x,y)$ and they are defined as follows.

$$n_{1p}(z,t) = \int_{\Omega_d} N_1(x,y,z,t)\, i_p(x,y)\, dxdy \tag{4a}$$

$$n_{3p}(z,t) = \int_{\Omega_d} N_3(x,y,z,t)\, i_p(x,y)\, dxdy \tag{4b}$$

$$n_{4p}(z,t) = \int_{\Omega_d} N_4(x,y,z,t)\, i_p(x,y)\, dxdy \tag{4c}$$

$$n_{6p}(z,t) = \int_{\Omega_d} N_6(x,y,z,t)\, i_p(x,y)\, dxdy \tag{4d}$$

$$n_{3s}(z,t) = \int_{\Omega_d} N_3(x,y,z,t)\, i_s(x,y)\, dxdy \tag{4e}$$

$$n_{4s}(z,t) = \int_{\Omega_d} N_4(x,y,z,t)\, i_s(x,y)\, dxdy \tag{4f}$$

These coefficients allow to take into account the overlapping strength between the spatial distribution of ion populations and the electromagnetic field.

To solve (3), the following initial conditions are imposed.

$$P_p(0,t) = P_p^{in}(t) \tag{5a}$$

$$P_s^+(0,t) = R_1 P_s^-(0,t) \tag{5b}$$

$$P_s^-(0,t) = R_2 P_s^+(L,t) \tag{5c}$$

where $z=0$ and $z=L$ represent the ends of the laser cavity, $P_{p0}(t)$ is the input pump power, R_1 and R_2 are the first and second mirror reflectivity, respectively. Time initial conditions are also considered as follows.

$$N_1(x,y,z,0) = N_{tot}(x,y,z) \tag{5d}$$

$$N_2(x,y,z,0) = N_3(x,y,z,0) = N_4(x,y,z,0) = N_5(x,y,z,0) = N_6(x,y,z,0) = 0 \tag{5e}$$

$$P_p(z,0) = P_s^+(z,0) = P_s^-(z,0) = 0 \tag{5f}$$

To evaluate the time evolution of the generated pulses, the output power is defined as

$$P_s^{out}(t) = [1 - R_2(\nu_s)]\, P_s^+(L,t) \tag{6}$$

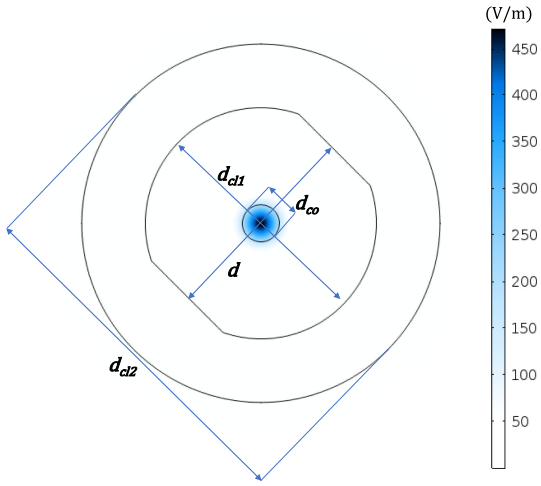

Fig. 2. Double-cladding fluoroindate fiber section geometry with the electric field modulus (V/m), arbitrarily normalized, of the fundamental HE_{11} mode.

III. Pulsed Laser Design

The considered fiber is a step-index double-cladding fluoroindate (InF_3) glass fiber, doped with 10 mol.% of Ho^{3+} ions, commercially available by Le Verre Fluoré [17]. The core diameter is $d_{co} = 16\ \mu$m and the numerical aperture $NA = 0.2$.

The cladding is 2-D shaped, obtained with circular diameter $d_{cl1} = 100\ \mu$m truncated by two parallel plans at a distance $d = 90\ \mu$m, to enhance cladding pump absorption. The second cladding has diameter $d_{cl2} = 155\ \mu$m. Fig. 2 illustrates the fiber section geometry and the electric field modulus of the fundamental HE_{11} mode simulated via a Finite Element Method (FEM) code. The aforesaid fiber is slightly multimode with normalized frequency number $V = 2.56$ at the signal wavelength. It exhibits a second order mode, which can be neglected in the laser operation since its overlapping coefficient with the spatial distribution of ion populations is less than a half of that pertaining to the fundamental mode. This prevents its contribution in the laser operation.

The rare earth dopant concentration is $N_{Ho} = 100\ 000\ ppm = 2 \times 10^{27}\ ions/m^3$. The used spectroscopic and optical parameters are taken from [28], [29] and listed in Table I. Since ETU rate K, cross relaxation (CR_1) rate W_{CR1}, and cross relaxation (CR_2) rate W_{CR2} are reported in literature with respect to relative level populations, they were obtained by dividing the values of [28], [29] by the dopant concentration N_{Ho}. The pump and signal wavelengths are $\lambda_p = 888\ nm$ and $\lambda_s = 3920\ nm$, respectively. The equivalent ASE noise bandwidth is $B_{ase} = 100\ nm$, while the optical losses are $\alpha = 0.2$ dB/m for both pump and signal wavelengths as reported in [30]. The simulations are performed via the differential equations by using Finite-Difference Time-Domain (FDTD) method, by considering a time grid with step $\Delta t = 0.1$ ns and a space grid with step Δz to obtain twenty space samples along the fiber. The pump excitation waveform is considered as a square wave with amplitude P_p^{peak}, repetition rate f, and duty cycle D.

TABLE I
SPECTROSCOPIC PARAMETERS OF FLUOROINDATE GLASS FIBER [28], [29]

Symbol	Value	Description
$\sigma_{14}(\lambda_p)$	$4.3 \times 10^{-26}\ m^2$	Absorption cross section $I_8 \rightarrow I_5$
$\sigma_{41}(\lambda_p)$	$4.3 \times 10^{-26}\ m^2$	Emission cross section $I_5 \rightarrow I_8$
$\sigma_{36}(\lambda_p)$	$7.1 \times 10^{-25}\ m^2$	Absorption cross section $I_6 \rightarrow S_2$
$\sigma_{63}(\lambda_p)$	$7.1 \times 10^{-25}\ m^2$	Emission cross section $S_2 \rightarrow I_6$
$\sigma_{34}(\lambda_s)$	$3.4 \times 10^{-25}\ m^2$	Absorption cross section $I_6 \rightarrow I_5$
$\sigma_{43}(\lambda_s)$	$3.4 \times 10^{-25}\ m^2$	Emission cross section $I_5 \rightarrow I_6$
τ_{R2}	$16.2\ ms$	I_7 radiative lifetime
τ_{R3}	$6.2\ ms$	I_6 radiative lifetime
τ_{R4}	$135\ \mu s$	I_5 radiative lifetime
τ_{R5}	$16.3\ \mu s$	F_5 radiative lifetime
τ_{R6}	$312\ \mu s$	S_2 radiative lifetime
β_{21}	1	$I_7 \rightarrow I_8$ branching ratio
β_{31}	0.942	$I_6 \rightarrow I_8$ branching ratio
β_{32}	0.058	$I_6 \rightarrow I_7$ branching ratio
β_{41}	0.557	$I_5 \rightarrow I_8$ branching ratio
β_{42}	0.430	$I_5 \rightarrow I_7$ branching ratio
β_{43}	0.013	$I_5 \rightarrow I_6$ branching ratio
β_{51}	0.758	$F_5 \rightarrow I_8$ branching ratio
β_{52}	0.192	$F_5 \rightarrow I_7$ branching ratio
β_{53}	0.046	$F_5 \rightarrow I_6$ branching ratio
β_{54}	0.004	$F_5 \rightarrow I_5$ branching ratio
β_{61}	0.500	$S_2 \rightarrow I_8$ branching ratio
β_{62}	0.400	$S_2 \rightarrow I_7$ branching ratio
β_{63}	0.100	$S_2 \rightarrow I_6$ branching ratio
β_{64}	≈ 0	$S_2 \rightarrow I_5$ branching ratio
β_{65}	≈ 0	$S_2 \rightarrow F_5$ branching ratio
K	$2.11 \times 10^{-24}\ m^3/s$	Energy transfer upconversion (ETU) rate
W_{CR1}	$3.48 \times 10^{-23}\ m^3/s$	Cross relaxation (CR1) rate
W_{CR2}	$1.5 \times 10^{-22}\ m^3/s$	Cross relaxation (CR2) rate

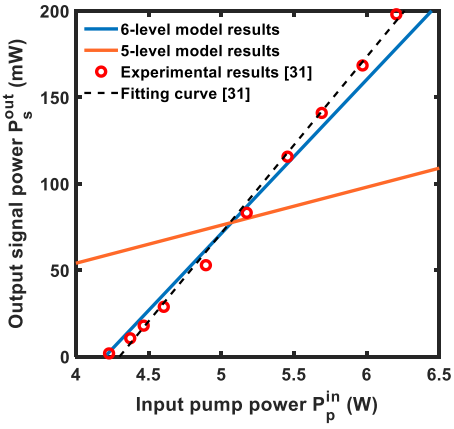

Fig. 3. Output signal power P_s^{out} as a function of the input pump power P_p^{in}, for the six-level model (blue line), five-level model (orange line), experimental results (red circles) [31], and the fitting linear line for the experimental results (black dashed line) [31].

A. Model Validation

The six-level model is validated by considering the experimental data reported in literature [31]. In particular, Fig. 3 shows the comparison between the six-level model and of the five-level model simulated efficiencies, with respect to the measured values, for a CW input pump, i.e., for a duty cycle $D = 100\%$, fiber length $L_{fiber} = 23$ cm, and second mirror reflectivity $R_2 = 84\%$ [31]. A slope efficiency $\eta_{CW} = 8.9\%$ and power threshold $P_{th} = 4.2\ W$ are simulated with the six-level model. These values are in good agreement with the experimental ones $\eta_{CW} = 10.2\%$ and $P_{th} = 4.3\ W$. The five- level model provides less accurate simulation results, the slope efficiency being $\eta_{CW} = 2.27\%$ and the power threshold $P_{th} = 1.5\ W$ with a significant deviation with respect to the experimental values. The discrepancy between the experimental values and the six-level model simulated parameters could be due to i) the employed attenuation $\alpha = 0.2$ dB/m for both pump and signal wavelengths, which is probably overestimated and ii) the employed emission and absorption cross-section approximated as coincident at the two considered wavelengths, listed in Table I. However, in absence of further experimental spectroscopic data, we keep this choice which is precautionary for the laser feasibility investigation.

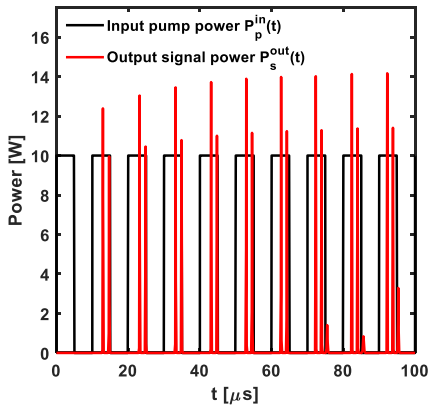

Fig. 4. Output signal pulses (red curve) and input pump pulses (black curve), with peak power $P_p^{peak} = 10\ W$, as a function of time. Pump repetition rate $f = 100$ kHz, input pump duty cycle $D = 50\%$, fiber length $L_{fiber} = 10$ cm, second mirror reflectivity $R_2 = 70\%$.

B. Pulsed Laser Results

As an example of the pulsed laser simulation, Fig. 4 shows the unregular output signal pulses $P_s^{out}(t)$ (red curve) at the end of the fiber length L_{fiber} and the input pump pulses $P_p^{in}(t)$ (black curve), with peak power $P_p^{peak} = 10\ W$, as a function of time t; pump repetition rate $f = 100$ kHz, input pump duty cycle $D = 50\%$, fiber length $L_{fiber} = 10$ cm, and second mirror reflectivity $R_2 = 70\%$. In the simulation, the considered input pump laser is the effectively coupled in the fiber. The laser of Fig. 4 is not optimized. The emission exhibits multiple output peaks with unstable amplitudes.

A deep investigation about the dependence of the laser output signal peak power P_s^{peak}, output signal pulse width τ_s, and energy E_s, on the laser fiber length L_{fiber} for different pairs of input pump duty cycle D and second mirror reflectivity R_2, (see Figs. 5 – 7) is carried out. Since variations of the input pump duty cycle D and of the second mirror reflectivity R_2 are strictly related, they have been investigated simultaneously. After a high number of simulations, only the cases of practical interest, with stable single pulse operation, are reported. For all investigated

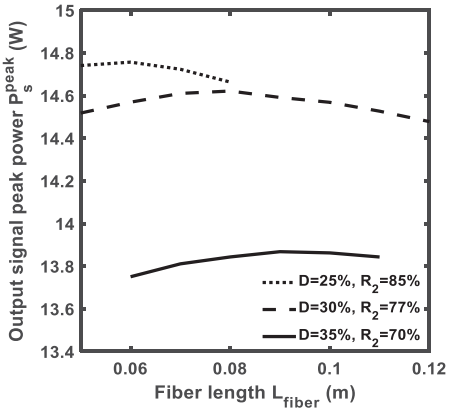

Fig. 5. Output signal peak power P_s^{peak} as a function of the laser fiber length L_{fiber}, for different pairs of input pump duty cycle D and second mirror reflectivity R_2. Pump repetition rate $f = 100$ kHz.

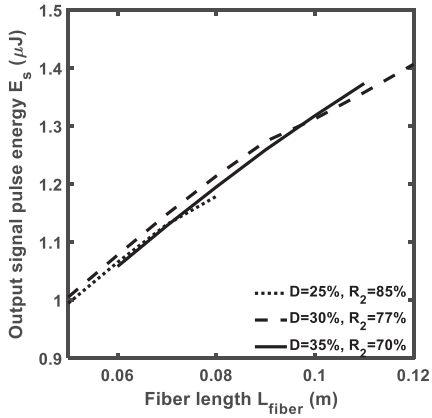

Fig. 7. Output signal pulse energy E_s as a function of the laser fiber length L_{fiber} , for different pairs of input pump duty cycle D and second mirror reflectivity R_2. Pump repetition rate $f = 100$ kHz.

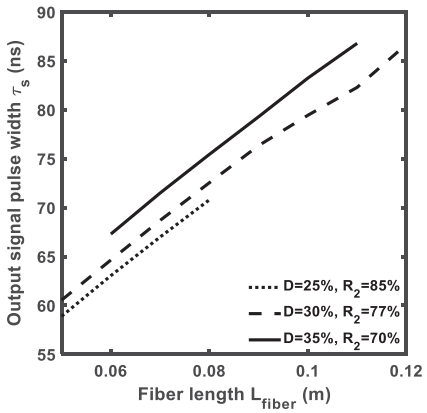

Fig. 6. Output signal pulse width τ_s as a function of the laser fiber length L_{fiber}, for different pairs of input pump duty cycle D and second mirror reflectivity R_2. Pump repetition rate $f = 100$ kHz.

cases, the output residual pump peak power was under the 1% of the input pump peak power.

Fig. 5 shows the output signal peak power P_s^{peak} as a function of the laser fiber length L_{fiber}, for different pairs of input pump duty cycle D and second mirror reflectivity R_2; pump repetition rate $f = 100$ kHz. As the input pump duty cycle D increases, the second mirror reflectivity R_2 must be reduced to guarantee single pulse output. This induces a strong decrease of the output signal peak power P_s^{peak}. The maximum output signal peak power $P_s^{peak} = 14.76\ W$ is obtained for the fiber length $L_{fiber} = 6$ cm, with input pump duty cycle $D = 25\%$ and second mirror reflectivity $R_2 = 85\%$.

Fig. 6 shows the output signal pulse full width at half maximum (FWHM) width τ_s as a function of the laser fiber length L_{fiber}, for different pairs of input pump duty cycle D and second mirror reflectivity R_2; pump repetition rate $f = 100$ kHz. The output pulse width τ_s increases almost linearly with the fiber length L_{fiber}. It is weakly dependent on the input pump duty cycle D and the second mirror reflectivity R_2. To shorten the output optical pulse duration, reduced fiber lengths L_{fiber} are more suitable. The shortest output pulse width $\tau_s = 58.9$ ns is obtained for input pump duty cycle $D = 25\%$, second mirror reflectivity $R_2 = 85\%$, and fiber length $L_{fiber} = 5$ cm. This small length value is feasible thank to the very high dopant concentration.

Fig. 7 shows the output signal pulse energy E_s as a function of the laser fiber length L_{fiber}, for different pairs of input pump duty cycle D and second mirror R_2; pump repetition rate $f = 100$ kHz. It grows almost linearly with the fiber length L_{fiber} and it is quite independent from the input pump duty cycle D and the second mirror reflectivity R_2. The maximum output signal pulse energy $E_s = 1.37\ \mu$J is obtained for the input pump duty cycle $D = 30\%$, second mirror reflectivity $R_2 = 77\%$, and fiber length $L_{fiber} = 12$ cm, leading to an optical-to-optical internal efficiency $\eta = 4.57\%$. The fiber length $L_{fiber} = 5$ cm allows the shortest obtained pulse width τ_s but leads to the minimum output signal pulse energy E_s. To find a tradeoff among the output signal peak power P_s^{peak} as high as possible, the output signal pulse width τ_s as short as possible, and the output signal pulse energy E_s as high as possible, the combination $R_2 = 77\%$ and $L_{fiber} = 8$ cm is chosen for the next investigations.

The investigation is completed by considering the dependence of the laser output signal peak power P_s^{peak}, output signal pulse width τ_s, and energy E_s on the input pump duty cycle D, for different values of the pump repetition rate f (see Figs. 8–10).

Fig. 8 shows the output signal peak power P_s^{peak} as a function of the input pump duty cycle D, for different values of the pump repetition rate f; fiber length $L_{fiber} = 8$ cm; second mirror reflectivity $R_2 = 77\%$, input pump peak power $P_p^{peak} = 10\ W$. The domains of correct laser operation are very narrow and strongly discontinuous. For each value of f only a small variation of D is allowed in order to obtain a stable single pulse output. Moreover, as the pump repetition rate f increases, also the input pump duty cycle D must increase to obtain the correct pulsed laser operation with stable single pulse output. The output signal peak power P_s^{peak} slightly increases, varying from $P_s^{peak} = 14.5\ W$ to $P_s^{peak} = 14.87\ W$, as f and D increase.

Fig. 9 shows the output signal pulse width τ_s as a function of the input pump duty cycle D, for different values of the pump

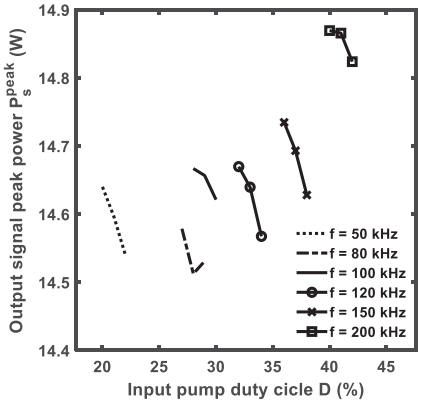

Fig. 8. Output signal peak power P_s^{peak} as a function of the input pump duty cycle D, for different values of the pump repetition rate f. Fiber length $L_{fiber} = 8$ cm, second mirror reflectivity $R_2 = 77\%$.

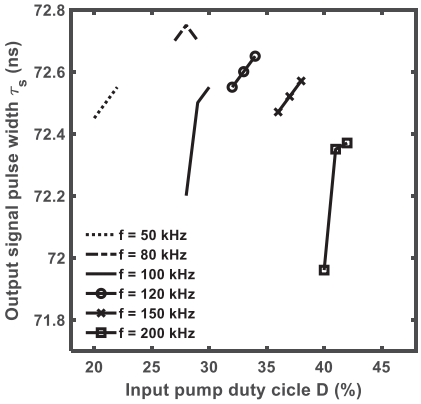

Fig. 9. Output signal pulse width τ_s as a function of the input pump duty cycle D, for different values of the pump repetition rate f. Fiber length $L_{fiber} = 8$ cm, second mirror reflectivity $R_2 = 77\%$.

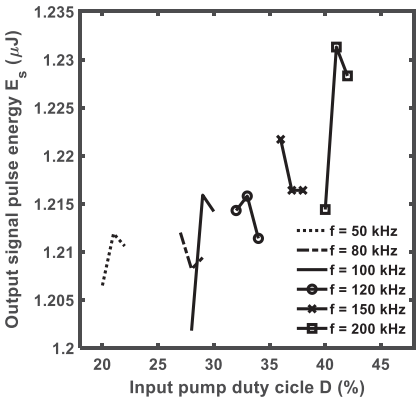

Fig. 10. Output signal pulse energy E_s as a function of the input pump duty cycle D, for different values of the pump repetition rate f. Fiber length $L_{fiber} = 8$ cm, second mirror reflectivity $R_2 = 77\%$.

repetition rate f; fiber length $L_{fiber} = 8$ cm , second mirror reflectivity $R_2 = 77\%$. The output signal pulse width τ_s slightly decreases by increasing the pump repetition rate f and the input pump duty D, changing from $\tau_s = 72.75$ ns to $\tau_s = 71.9$ ns.

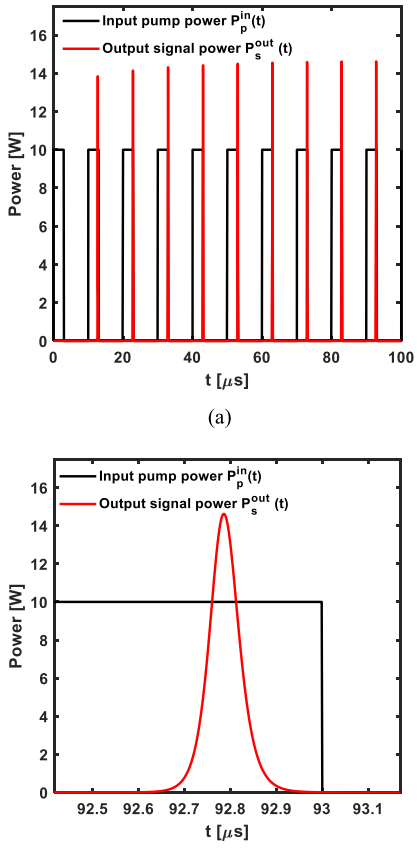

Fig. 11. (a) Output signal pulses (red curve) and the input pump pulses (black curve), with peak power $P_p^{peak} = 10\ W$, as a function of time. Pump repetition rate $f = 100$ kHz, input pump duty cycle $D = 30\%$, fiber length $L = 8$ cm, second mirror reflectivity $R_2 = 77\%$. (b) Zoom of a single output signal pulse.

Fig. 10 shows the output signal pulse energy E_s as a function of the input pump duty cycle D, for different values of the pump repetition rate f; fiber length $L_{fiber} = 8$ cm, second mirror reflectivity $R_2 = 77\%$. The output signal pulse energy E_s exhibits a small increasement as the pump repetition rate f and the input pump duty D increase. It is $E_s = 1.207$ μJ for $f = 50$ kHz and $D = 20\%$ and $E_s = 1.23$ μJ for $f = 200$ kHz and $D = 41\%$. This investigation predicts that good laser performances can be obtained till $f = 200$ kHz also by varying the pump repetition rate in the whole investigated range, promising great flexibility of the proposed device.

Lastly, the output signal pulses $P_s^{out}(t)$ (red curve) and the input pump pulses $P_p^{in}(t)$ (black curve), with peak power $P_p^{peak} = 10\ W$, as a function of time t, for the optimized cavity is illustrated in Fig. 11 for the pump repetition rate $f = 100$ kHz, duty cycle $D = 30\%$, fiber length $L_{fiber} = 8$ cm, output mirror reflectivity $R_2 = 77\%$. A stable single pulse signal at $\lambda_s = 3.92$ μm with an output signal peak power $P_s^{peak} = 14.62\ W$, pulse width $\tau_s = 72.55$ ns, signal pulse energy $E_s = 1.214$ μJ and optical-to-optical internal efficiency $\eta = 4.05\%$ is obtained. The time to first pulse is $t_{fp} = 15$ μs and the stable gain-switched regime is achieved after about $t_R = 60$ μs. The obtained efficiency is consistent with the CW laser one [31].

These results pave the way to fabricate a new pulsed laser, based on a commercially available fluoroindate fiber, with a stable output in a wide range of repetition pump rates f, from $f = 50$ kHz to beyond 200 kHz. We underline that, due to the narrow domains in which the laser exhibits stable single pulse operation, the optimized laser parameters, identified in the proposed design, provide useful guidelines to be followed in order to obtain a feasible pulsed emission. The interest is also due to the potential optimizations which could be obtained by co-doping the fluoroindate fiber with Ho^{3+} and Nd^{3+} ions and employing a pumping scheme at $\lambda_p = 808\ nm$ [38].

IV. Conclusion

For the first time, a pulsed laser emitting at $\lambda_s = 3.92\ \mu$m based on a commercial double-cladding heavily holmium-doped fluoroindate glass fiber is accurately designed via a validated model, by using measured spectroscopic parameters. By employing an input pump with peak power $P_p^{peak} = 10\ W$ at the wavelength $\lambda_p = 888\ nm$, repetition rate $f = 100$ kHz and duty cycle $D = 30\%$, stable output pulses having peak power $P_s^{peak} = 14.62\ W$, pulse width FWHM $\tau_s = 72.55$ ns and pulse energy $E_s = 1.214\ \mu$J, are simulated. The proposed gain-switched laser enables stable pulsed output in a wide range of pump repetition rates, from $f = 50$ kHz to beyond $f = 200$ kHz. Future development will include different co-doping and pumping scheme solutions.

References

[1] D. D. Hudson, "Short pulse generation in mid-IR fiber lasers," *Opt. Fiber. Technol.*, vol. 20, no. 6, pp. 631–641, Dec. 2014.

[2] Q. Luo *et al.*, "Remote sensing of pollutants using femtosecond laser pulse fluorescence spectroscopy," *Appl. Phys. B*, vol. 82, pp. 105–109, Nov. 2005.

[3] A. Y. Sajjadi, K. Mitra, and M. Grace, "Ablation of subsurface tumors using an ultra-short pulse laser," *Opt. Lasers Eng.*, vol. 49, no. 3, pp. 451–456, Mar. 2011.

[4] L. Romoli, G. Lazzini, A. H. A. Lutey, and F. Fuso, "Influence of ns laser texturing of AISI 316L surfaces for reducing bacterial adhesion," *CIRP Ann.*, vol. 69, no. 1, pp. 529–532, 2020.

[5] A. E. Klingbeil, J. B. Jeffries, and R. K. Hanson, "Temperature-dependent mid-IR absorption spectra of gaseous hydrocarbons," *J. Quant. Spectrosc. Radiat. Transf.*, vol. 107, no. 3, pp. 407–420, Oct. 2007.

[6] J. M. Bakker *et al.*, "The mid-IR absorption spectrum of gas-phase clusters of the nucleobases guanine and cytosine," *Phys. Chem. Chem. Phys.*, vol. 6, no. 10, pp. 2810–2815, Apr. 2004.

[7] K. Wang, D.-W. Sun, and H. Pu, "Emerging non-destructive terahertz spectroscopic imaging technique: Principle and applications in the agri-food industry," *Trends Food Sci. Technol.*, vol. 67, pp. 93–105, Sep. 2017.

[8] M. C. Falconi, D. Laneve, M. Bozzetti, T. T. Fernandez, G. Galenzano, and F. Prudenzano, "Design of an efficient pulsed Dy^{3+}: ZBLAN fiber laser operating in gain switching regime," *J. Lightw. Technol.*, vol. 36, no. 23, pp. 5327–5333, Sep. 2018.

[9] X. Jin *et al.*, "High-power ultralong-wavelength Tm-doped silica fiber laser cladding-pumped with a random distributed feedback fiber laser," *Sci. Rep.*, vol. 6, Jul. 2016, Art. no. 30052.

[10] E. A. Anashkina, "Laser sources based on rare-earth ion doped tellurite glass fibers and microspheres," *Fibers*, vol. 8, no. 30, pp. 1–17, May 2020.

[11] M. C. Falconi *et al.*, "Dysprosium-doped chalcogenide master oscillator power amplifier (MOPA) for mid-IR emission," *J. Lightw. Technol.*, vol. 35, no. 2, pp. 265–273, Jan. 2017.

[12] M. R. Majewski, R. I. Woodward, J.-Y. Carrée, S. Poulain, M. Poulain, and S. D. Jackson, "Emission beyond 4 μm and mid-infrared lasing in a dysprosium-doped indium fluoride (InF_3) fiber," *Opt. Lett.*, vol. 43, no. 8, pp. 1926–1929, 2018.

[13] M. C. Falconi, D. Laneve, V. Portosi, S. Taccheo, and F. Prudenzano, "Design of a multi-wavelength fiber laser based on tm:Er:Yb:Ho co-doped germanate glass," *J. Lightw. Technol.*, vol. 38, no. 8, pp. 2406–2413, Jan. 2020.

[14] P. Paradis, V. Fortin, Y. O. Aydin, R. Vallée, and M. Bernier, "10 W-level gain-switched all-fiber laser at 2.8 μm," *Opt. Lett.*, vol. 43, no. 13, pp. 3196–3199, Jul. 2018.

[15] F. Jobin, V. Fortin, F. Maes, M. Bernier, and R. Vallée, "Gain-switched fiber laser at 3.55 μm," *Opt. Lett.*, vol. 43, no. 8, pp. 1770–1773, Apr. 2018.

[16] N. Bawden *et al.*, "Actively Q-switched dual-wavelength pumped Er3+:ZBLAN fiber laser at 3.47 μm," *Opt. Lett.*, vol. 43, no. 11, pp. 2724–2727, Jun. 2018.

[17] Le Verre Fluoré, Catalog 2019, Bruz, Brittany, France. [Online]. Available: https://leverrefluore.com/wp-content/uploads/2019/06/CatalogLVF-2019.pdf

[18] M. Saad, R. Pafchek, P. Foy, Z. Jiang, D. Gardner, and P. Hawkins, "Indium fluoride glass fibers for mid-infrared applications," in *Proc. WSOF2015*, Hong Kong, China, 2015, Paper WW4A.3.

[19] J. Pisarska, "IR transmission and emission spectra of erbium ions in fluoroindate glass," *J. Non-Cryst. Solids*, vol. 345-346, pp. 382–385, Oct. 2004.

[20] V. A. Jerez, C. B. de Araujo, and Y. Messaddeq, "Dynamics of energy transfer and frequency upconversion in Tm^{3+} doped fluoroindte glass," *J. Appl. Phys.*, vol. 96, no. 5, pp. 2530–2534, Sep. 2004.

[21] D. Manzani, D. Paboeuf, S. J. L. Ribeiro, P. Goldner, and F. Bretenaker, "Orange emission in Pr^{3+}-doped fluoroindate glasses," *Opt. Mater.*, vol. 35, no. 3, pp. 383–386, Jan. 2013.

[22] L. J. Borrero-Gonzalez, G. Galleani, D. Manzani, L. A. O. Nunes, and S. J. L. Ribeiro, "Visible to infrared energy conversion in Pr^{3+}- Yb^{3+} co-doped fluoroindate glasses," *Opt. Mater.*, vol. 35, no. 12, pp. 2085–2089, Oct. 2013.

[23] M. Kochanowicz *et al.*, "Near-IR and mid-IR luminescence end energy transfer in fluoroindate glasses co-doped with Er^{3+}/Tm^{3+}," *Opt. Mater. Exp.*, vol. 9, no. 12, Dec. 2019.

[24] M. Kochanowicz *et al.*, "Sensitization of Ho^{3+}-doped fluoroindate glasses for near and mid-infrared emission," *Opt. Mater.*, vol. 101, Mar. 2020, Art. no. 109707.

[25] A. Florez, S. L. Oliveira, M. Florez, L. A. Gomez, and L. A. O. Nunes, "Spectroscopic characterization of Ho^{3+} ion-doped fluoride glass," *J. Alloys Compd.*, vol. 418, pp. 238–242, Feb. 2006.

[26] S. L. Oliveira, M. J. V. Bell, A. Florez, and L. A. O. Nunes, "Spectroscopic investigation of 2.0 μm emission in Ho^{3+}-doped fluoroindate glasses," *J. Phys. D: Appl. Phys.*, vol. 39, pp. 3230–3234, Jul. 2006.

[27] A. Berrou, C. Kieleck, and M. Eichhorn, "Mid-infrared lasing from Ho^{3+} in bulk inf_3 glass," *Opt. Lett.*, vol. 40, no. 8, pp. 1699–1701, Apr. 2015.

[28] L. Gomes *et al.*, "The basic spectroscopic parameters of Ho^{3+}-doped fluoroindate glass for emission at 3.9 μm," *Opt. Mater.*, vol. 60, pp. 618–626, Sep. 2016.

[29] L. Gomes *et al.*, "Excited state absorption and energy transfer in Ho^{3+}-doped indium fluoride glass," *Opt. Mater.*, vol. 66, pp. 519–526, Feb. 2017.

[30] S. Jia *et al.*, "2875 nm Lasing from Ho^{3+}-Doped fluoroindate glass fibers," *IEEE Photon. Technol. Lett.*, vol. 30, no. 4, pp. 323–326, Feb. 2018.

[31] F. Maes *et al.*, "Room-temperature fiber laser at 3.92 μm," *Optica*, vol. 5, no. 7, pp. 761–764, Jul. 2018.

[32] F. Zhou, J. Li, H. Luo, F. Quellette, and Y. Liu, "Numerical analysis of 3.92 μm dual-wavelength pumped heavily-holmium-doped fluoroindate fiber lasers," *J. Lightw. Technol*, vol. 39, no. 2, pp. 633–645, Jan. 2021.

[33] K. S. Wu, D. Ottaway, J. Munch, D. G. Lancaster, S. Bennetts, and S. D. Jackson, "Gain-switched holmium-doped fibre laser," *Opt. Exp.*, vol. 17, no. 23, pp. 20872–20877, Nov. 2009.

[34] J. Li, Y. Yang, D. D. Hudson, Y. Liu, and S. D. Jackson, "A tunable Q-switched Ho^{3+}-doped fluoride fiber laser," *Laser Phys. Lett.*, vol. 10, Feb. 2013.

[35] H. Luo, Y. Xu, J. Li, and Y. Liu, "Gain-switched dysprosium fiber laser tunable from 2.8 to 3.1 μm," *Opt. Exp.*, vol. 27, no. 19, Sep. 2019.

[36] L. Pajewski, L. Sojka, S. Lamrini, T. M. Benson, A. B. Seddon, and S. Sujecki, "Gain-switched Dy^{3+}:ZBLAN fiber laser operating around 3 μm," *J. Phys. Photon.*, vol. 2, no. 1, Jan. 2020, Art. no. 014003.

[37] G. Palma *et al.*, "Design of praseodymium-doped chalcogenide micro-disk emitting at 4.7 μm," *Opt. Exp.*, vol. 25, no. 6, pp. 7014–7030, Mar. 2017.

[38] R. Wang *et al.*, "3.9 μm emission and energy transfer in ultra-low OH–, Ho^{3+}/Nd^{3+} co-doped fluoroindate glasses," *J. Lumin.*, vol. 225, Sep. 2020, Art. no. 117363.

Antonella Maria Loconsole received the M.Sc. degree in 2019 in telecommunications engineering (cum laude) from Politecnico di Bari, Bari, Italy, where she is currently working toward the Ph.D. degree in electrical and information engineering. Her research interests include SIW antennas, microwave applicators for medical applications, and optical fiber lasers and amplifiers.

Mario Christian Falconi received the M.Sc. degree in electronic engineering (cum laude) and the Ph.D. degree in electrical and information engineering from Politecnico di Bari, Bari, Italy, in 2015 and 2019, respectively. In 2019, he was a Research Fellow and is currently a Research Assistant in electromagnetic fields with the Department of Electrical and Information Engineering, Polytechnic University of Bari, Bari, Italy. His research interests include fiber lasers and amplifiers, photonic crystal fibers, and nonlinear effects in optical fibers.

Vincenza Portosi received the M.Sc. degree in 2018 in electronic engineering (cum laude) from Politecnico di Bari, Bari, Italy, where she is currently working toward the Ph.D. degree in electrical and information engineering. Her research interests include microwave applicators for medical applications, metamaterials, SIW antennas, and optical fiber sensors.

Francesco Prudenzano (Member, IEEE) received the Ph.D. degree in electronic engineering from Politecnico di Bari, Bari, Italy, in November 1996. Since 2018, he has been a Full Professor in electromagnetic fields with the Department of Electrical and Information Engineering, Politecnico di Bari, Bari, Italy. His research interests include the design and characterization of microwave devices, integrated optics, and optical fiber-based devices. He is currently the Head of Microwave and Optical Engineering Group, Department of Electrical and Information Engineering, Politecnico di Bari. From 2017 to 2018, he was the Chair of SIOF, the Italian Society of Optics and Photonics (Italian branch of EOS - European Optical Society). He is involved in several national and international research projects and cooperations. He has coauthored more than 400 publications, 295 of which got published in journals and international conferences, lectures, and invited papers.